# Interfacial Shear at the Atomic Scale

**Martin Rejhon**
New York University Tandon School of Engineering
**Francesco Lavini**
New York University Tandon School of Engineering
**Ali Khosravi**
International School for Advance Studies (SISSA)
**Mykhailo Shestopalov**
Charles University, Faculty of Mathematics and Physics, Institute of Physics
**Jan Kunc**
Charles University, Faculty of Mathematics and Physics, Institute of Physics
**Erio Tosatti**
International School for Advanced Studies
**Elisa Riedo** ( elisa.riedo@nyu.edu )
New York University https://orcid.org/0000-0002-2423-8801

**Article**

**Keywords:** single atomic layer, shear modulus, shear stiffness

**Posted Date:** November 23rd, 2021

**DOI:** https://doi.org/10.21203/rs.3.rs-1051183/v1



**Version of Record:** A version of this preprint was published at Nature Nanotechnology on October 31st, 2022. See the published version at https://doi.org/10.1038/s41565-022-01237-7.

# Interfacial Shear at the Atomic Scale

Martin Rejhon[1], Francesco Lavini[1], Ali Khosravi[2,3,4], Mykhailo Shestopalov[5], Jan Kunc[5], Erio Tosatti[2,3,4], Elisa Riedo[1*]

[1] Tandon School of Engineering, New York University, Brooklyn, NY, 11201, USA

[2] International School for Advanced Studies (SISSA), Via Bonomea 265, 34136 Trieste, Italy

[3] The Abdus Salam International Centre for Theoretical Physics (ICTP), Strada Costiera 11, 34151 Trieste, Italy

[4] CNR-IOM, Consiglio Nazionale delle Ricerche - Istituto Officina dei Materiali, c/o SISSA, Via Bonomea 265, 34136 Trieste, Italy

[5] Charles University, Faculty of Mathematics and Physics, Institute of Physics, Ke Karlovu 5, CZ-121 16 Prague 2, Czech Republic

[*] Corresponding author: elisa.riedo@nyu.edu

Understanding the interfacial properties between an atomic layer and its substrate is of key interest at both the fundamental and technological level. From Fermi level pinning to strain engineering and superlubricity, the interaction between a single atomic layer and its substrate governs electronic, mechanical, and chemical properties of the layer-substrate system. Here, we measure the hardly accessible interfacial transverse shear modulus of an atomic layer on a substrate. We show that this key interfacial property is critically controlled by the chemistry, order, and structure of the atomic layer-substrate interface. In particular, the experiments demonstrate that the interfacial shear modulus of epitaxial graphene on SiC increases for bilayer films compared to monolayer films, and augments when hydrogen is intercalated between graphene and SiC. The increase in shear modulus for two layers compared to one layer is explained in terms of layer-layer and layer-substrate stacking order, whereas the increase with H-intercalation is correlated with the pinning induced by the H-atoms at the interface. Importantly, we also demonstrate that this modulus is a pivotal measurable property to control and predict sliding friction in supported two-dimensional materials. Indeed, we observe an inverse relationship between friction and interfacial shear modulus, which naturally emerges from simple friction models based on a point mass driven over a periodic potential. This inverse relation originates from a decreased dissipation in presence of large shear stiffness, which reduces the energy barrier for sliding.

Two-dimensional (2D) materials, such as graphene, are usually exfoliated onto, or directly grown on a substrate. Since 2D films or flakes are only one or a few atoms thick, their interaction with the substrate is quite important. Indeed, substrate interaction can change 2D materials chemical, electronic, and mechanical properties[1-3]. Furthermore, intercalation of atoms between substrate and 2D layers is a common methodology to tune the properties of 2D films, including doping level and conductivity[4,5], interlayer friction[6], stiffness[7], catalytic activity[8], and optical properties[9]. Interlayer and layer-substrate interactions are usually probed by investigations of their electronic properties, e.g. angle-resolved photoemission spectroscopy (ARPES)[4], or by studying the presence of strain in the films by Raman spectroscopy[10,11]. Recently, interlayer elasticity has been probed by atomic force microscopy (AFM), and has shown a high sensitivity to the presence of intercalated water in graphene oxide[7].

An important property of the substrate/2D layer interface is the interfacial transverse (out-of-plane) shear modulus[12], $G_{int}$, measured from the in-plane strain experienced by the top atomic layer when a shear force, parallel to its surface, is applied to the atomic layer while the substrate experiences an opposing force (see Fig. 1a). This shear modulus, which is conceptually similar to the $C_{44}$ elastic modulus in graphite[13,14], is critically related to the chemistry, order, and structure of the interface[14], and it is of key importance to understand strain controlled electronic and optical properties[15], as well as the frictional behavior of 2D materials[16]. It is also relevant for a broad spectrum of applications, including nanomechanical and nanoelectromechanical systems[17-20], flexible electronics[21], and biology[22]. Unfortunately, there are very few theoretical and experimental studies on the transverse shear modulus of 2D multilayers[23,24], and no reported measurement or calculation of the interfacial transverse shear modulus of a single atomic layer on a substrate.

Here, we show how to measure and control the interfacial transverse shear modulus of supported one and two atomic layers on a substrate, (see Fig. 1a and Fig. S1-S8 in Supplementary Information (SI)). In particular, we investigate mono- and bi-layer epitaxial graphene on the conventional C-buffer layer on SiC (0001)[25] (Fig. 1b, left), as well as mono- and bi-layer quasi-free-standing epitaxial graphene on H-terminated SiC (0001)[26,27] (see Fig. 1b, right, Methods part and SI). We show that the interfacial shear modulus increases for bilayer films compared to monolayer films, in both systems, i.e., with and without hydrogen intercalation. However, interestingly, when H is intercalated between graphene and SiC, $G_{int}$ augments, and it is rigidly shifted towards higher values for both one and two layers. While the increase in $G_{int}$ for two layers compared to one layer can be related to layer-layer and layer-substrate stacking order, the increase after hydrogen intercalation is explained in terms of the

graphene layers being pinned by the H-atoms at the interface. Furthermore, we show that $G_{int}$ is a key physical and measurable property to control and predict sliding friction in supported 2D materials, a topic that has produced a large amount of fundamental yet somewhat controversial studies[1,28-35]. In particular, for the above-described cases of epitaxial graphene, we find an inverse relationship between friction and interfacial shear modulus, explained by the increased dissipation in presence of larger shear softness. Accordingly, we find that bilayer epitaxial graphene has a lower friction coefficient (larger shear modulus) than monolayer graphene, for both graphene on buffer layer and H-intercalated graphene. Moreover, after hydrogen intercalation the friction coefficient rigidly shifts, for both one and two layers, towards lower values, in agreement with the inverse friction/shear modulus relation. Specifically, single layer graphene sitting on H-terminated SiC, where H-atoms provide a stronger pinning of graphene on its substrate, has a higher $G_{int}$ and correspondingly lower friction than single layer graphene on buffer layer/SiC. These results can be easily understood, without invoking any other argument, with the simple Prandtl-Tomlinson model, which shows that for higher $G_{int}$ values, steady state friction has lower values due to a larger amount of energy stored elastically during the gradual sticking period, and a smaller amount of energy dissipated during the subsequent fast slipping. The model also shows that the sample with lower $G_{int}$ requires a larger energy barrier to initiate sliding compared to the sample with larger $G_{int}$. These findings are further rationalized by simplified one-dimensional simulations of a tip sliding over a Frenkel-Kontorova harmonic chain, which mimics the graphene layers, in presence of a sinusoidal "substrate" potential mimicking the shear stiffness of the substrate. An increase of substrate potential amplitude is related to an increase of interfacial shear stiffness. A lower shear stiffness – smaller potential amplitude – increases the tip-induced lateral deformation and associated dissipative events, resulting in a larger friction – a mechanism that differs from those proposed so far for 2D materials.

**Interfacial transverse shear modulus experiments**

The interfacial shear modulus of different types of epitaxial graphene films is here investigated by using a novel approach (Fig. S3 in SI), which is based on a modified version of the modulated nanoindentation (MoNI) method[7,36-38]. During a typical modulated nanoshear (MoNS) experiment, after a silicon AFM tip is brought into contact with a sample at a specific initial normal load ($F_N$ = 20 nN), the cantilever-holder is driven by a lock-in amplifier to oscillate parallel to the graphene surface, with a sub-Å oscillation amplitude ($\Delta x$ = 0.3 Å) (see Fig. 1a and SI). Because of such small oscillation amplitudes and the presence of adhesive forces,

during the oscillation the tip apex is always sticking to the surface of the sample (no slipping), and it induces a lateral shear in the underneath sample in a purely elastic regime, as shown in Fig. 1a. In this sticking regime, when static friction prevents the tip to slide, the force per unit displacement necessary to shear the top atomic layer in respect to the substrate is proportional to the effective interfacial shear modulus[39], $G^*_{int}$, defined as:

$$G^*_{int} = \left(\frac{2-\nu_{tip}}{G_{tip}} + \frac{2-\nu}{G_{int}}\right)^{-1}, \quad (1)$$

where $\nu_{tip}$ and $\nu$ are the Poisson's ratios, while $G_{tip}$ and $G_{int}$ are the interfacial transverse shear moduli of the AFM tip material and graphene sample, respectively. By measuring the lateral force ($\Delta F_L$) experienced by the cantilever during the oscillation $\Delta x$, while the tip is sticking into contact with the sample surface, it is possible to obtain the lateral stiffness of the tip-sample contact, $k_{cont}^{lateral}$, following the equation[39]

$$\frac{\Delta F_L}{\Delta x} = \left(\frac{1}{k_{lever}^t} + \frac{1}{k_{cont}^{lateral}}\right)^{-1} = k_{total}^{lateral}, \quad (2)$$

where $k_{lever}^t$ is the torsional spring constant of the AFM cantilever ($k_{lever}^t$ = 70.7 N/m), see SI. Furthermore, $G^*_{int}$ is related to $k_{cont}^{lateral}$ by the relationship:

$$k_{cont}^{lateral} = 8 G_{int}^* a, \quad (3)$$

where $a$ is the tip-sample contact radius, and $G^*_{int}$ is defined in Eq. (1). Contact mechanics equations[39] can then be used to calculate $a$ from the normal load and the adhesion force $F_{adh}$ :

$$a = \left(\frac{3R_{tip}}{4E^*}(F_N + F_{adh})\right)^{1/3}, \quad (4)$$

where $R_{tip}$ is the tip radius and E* is the effective Young modulus of the tip-sample contact (Eq. S4). During the MoNS experiments, $F_{adh}$ is directly measured from the $k_{cont}^{lateral}$ vs. load curves (Fig. 2) as the lowest load at which the contact is lost[7], while E* is measured via MoNI/AI for each sample (see Methods).

The lateral contact stiffness is measured at different decreasing loads, while retracting the tip from the initial contact load (20 nN), until complete detachment from the surface is achieved at $F_N = F_{adh}$. $G_{int}$ is then obtained by fitting the experimental $k_{cont}^{lateral}(F_N)$ curves with the following equation:

$$k_{cont}^{lateral} = 8\left(\frac{2-\nu_{tip}}{G_{tip}} + \frac{2-\nu}{G_{int}}\right)^{-1}\left(\frac{3R_{tip}}{4E^*}(F_N + F_{adh})\right)^{1/3}. \quad (5)$$

The above-described MoNS experiments are then performed on different epitaxial graphene films of different thickness. In particular, we investigate four different types of epitaxial graphene films, namely, 1-layer and 2-layer epitaxial graphene films on the carbon-buffer layer

(see 1L/Bfl/SiC in Fig. 1b, left panel), and hydrogen intercalated 1L and 2L quasi-free-standing epitaxial graphene films (see 1L/H-SiC in Fig. 1b, right panel), more details are reported in the Methods section. Figure 2a shows the measured $k_{cont}^{lateral}$ ($F_N$) curves, where the data points are from a single experiment, while the shaded areas represent the standard deviation for multiple experiments. The obtained values of $G_{int}$ are averaged and summarized in Fig. 3. The experiments reveal that $G_{int}$ in epitaxial graphene increases with increasing number of layers, from 188 MPa for 1L/Bfl/SiC graphene to 220 MPa for 2L/Bfl/SiC graphene. First of all, we notice that the obtained $G_{int}$ values are close to the values of the transverse shear modulus ($C_{44}$ constant) of bulk turbo graphite, where the layer stacking is random, i.e., between 180 and 350 MPa[14,40], and also close to the values of the interlayer shear modulus of non-supported multi-layer graphene, about 400 ± 250 MPa[24]. This observation suggests that the measured $G_{int}$ is not related to an extensive stretching of the interatomic bonds within the graphene layer, equivalent to the much stiffer in-plane shear modulus of graphene, about 0.5 TPa[41]. Secondly, we observe the same $G_{int}$ dependance on the number of layers in both non intercalated and H-intercalated graphene samples. The interfacial shear modulus of 1L/H-SiC and 2L/H-SiC is 211 MPa and 246 MPa, respectively. The ratio between $G_{int}$ of 1L and 2L is equal to 0.86 for both non-intercalated and intercalated graphene, which corresponds to an increase of 16% for 2L in respect to 1L. This identical layer dependence of $G_{int}$ with the number of layers suggests that the origin of this increase is the same in both intercalated and non-intercalated graphene. Density functional theory (DFT) calculations have shown that the transverse shear modulus ($C_{44}$) of graphitic systems depends on the stacking orientation of the layers, with the perfect stacking (hex-g, AB) exhibiting the highest shear modulus, while the lowest modulus is attributed to random stacking[14]. For bilayer epitaxial graphene, the AB (Bernal) stacking structure is indeed the energetically favorable geometry[42]. Whereas regarding monolayer graphene, in the case of 1L/Bfl/SiC, it is sitting on top of the buffer layer, which is a disordered mixture of $sp^2$ and $sp^3$ hybridization[42,43] and has a certain, relatively modest, degree of roughness. On the other hand, in H-intercalated samples, the first graphene layer sits on top of a H-terminated SiC surface[44], while the second layer is again forming an AB (Bernal) stacking structure with the underlying first layer[45]. Therefore, we argue that the stacking misorientation of 1L graphene either on buffer layer or on H-SiC is the origin of a decreased $G_{int}$ compared to the ordered AB stacking of 2L graphene.

While the decrease in interfacial shear modulus for 2L films compared to 1L films is thus understood in terms of stacking, the 31% increase in $G_{int}$ after hydrogen intercalation can be explained by a pinning effect. Raman spectroscopy (see SI) indicates that hydrogen

intercalation decreases the number of defects in the graphene films, suggesting that defects are not responsible for the pinning. Neither does adhesion energy, which remains basically the same after H-intercalation (see Supplementary Information Table 2). However, our data suggests that H-atoms at the interface actually provide a source of pinning more important than that of the buffer layer, and hinder the shear of the top atomic graphene layer. While H-atoms are predominantly attached to the SiC substrate, we cannot exclude that a very small portion of hydrogen is also attached to the bottom of the graphene layer, further increasing the pinning effect. We remark that in the case of 2L films on H-terminated SiC, the effect of the bottom layer hindered shear propagates to the top layer, increasing the overall shear stiffness of 2L/H-SiC compared to 2L/Bfl/SiC.

**Friction force experiments**

As mentioned earlier, the lateral stiffness of the contact between the 2D film and the tip sliding on top of it – which is proportional to $G^*_{int}$ – is intimately connected with the static and dynamic friction processes[39]. In particular, the interfacial shear modulus has a direct impact on the energy dissipation mechanisms underlying friction. However, previous studies have not considered the role of the interfacial shear modulus in understanding friction in 2D materials. So far, the well-known decrease in frictional forces when increasing the number of atomic layers in 2D materials has been attributed to either a puckering effect[31], or to phonon-electron coupling in epitaxial graphene[29]. Here, we show that the interfacial shear modulus is a key physical and measurable property to control sliding friction in supported 2D materials. To investigate the correlation between interfacial shear modulus and frictional dissipation when a nano-tip slides on top of a 2D supported film, we perform AFM friction force microscopy (FFM) measurements[35]. Friction forces are measured for two types of non-intercalated epitaxial graphene samples (namely 1L/BFl/SiC and 2L/Bfl/SiC) and two H-intercalated samples (namely 1L/H-SiC and 2L/H-SiC), as a function of varying normal load, from -10 nN to 50 nN. More details about the FFM experimental set up are available in the Methods section and Supplementary Information.

The AFM topography and friction force maps acquired on the graphene samples at a specific normal load ($F_N$ = 50 nN) are displayed in Fig. 4a. For each graphene sample, the friction forces $F_F$ are extracted from the friction maps. We remark that in each sample there are areas with different number of layers, as identified by the friction maps and Raman spectra. From the friction maps at different loads of the different areas of interest – highlighted by solid-line boundaries in Fig. 4a – we obtain and then plot the average friction force vs. normal load, as

displayed in Fig. 4b. We observe that 1L graphene shows higher friction than 2L epitaxial graphene. For example, at $F_N$ = 50 nN 1L/Bfl/SiC friction forces are around 1.5 times larger than 2L/Bfl/SiC, in good agreement with the literature data[28,29]. To date, the friction behavior of H-intercalated graphene has not been studied, to the best of our knowledge. As expected for the case of non-intercalated samples, also the friction forces of H-intercalated graphene decrease with increasing number of layers, for the entire range of applied normal loads. However, surprisingly, the friction forces rigidly decrease to lower values for H-intercalated graphene, for both 1L and 2L samples. Similarly, with what we find for the interfacial shear modulus, we observe the same friction force values for non-intercalated 2L/Bfl/SiC and intercalated 1L/H-SiC. To get a better understanding of the intrinsic frictional properties of the materials, we also calculate the friction coefficients, μ. By fitting the friction force curves in Fig. 4b with the power-law fitting curve described in Eq. 7 (see Method section), we derive the friction coefficient $\mu$ for the four types of graphene samples. In particular, we obtain a coefficient of $2.3\times10^{-2}$ $nN^{1/3}$ for 1L/Bfl/SiC, $1.4\times10^{-2}$ $nN^{1/3}$ for 2L/Bfl/SiC, $1.4\times10^{-2}$ $nN^{1/3}$ for 1L/H-SiC, and $0.9\times10^{-2}$ $nN^{1/3}$ for 2L/H-SiC. The values of the shear moduli and friction coefficients for the two pairs of non-intercalated and intercalated graphene are reported in Fig. 4c and summarized in the table depicted in Fig. 3. From Fig. 4c we can observe an inverse relationship between the interfacial shear modulus and the friction coefficient of the graphene samples, suggesting a correlation between the two physical parameters. The frictional behavior of 2D materials has been so far ascribed to the so-called puckering effect[1,31], electron-phonon (e-ph) coupling[29], surface roughness[46] and adhesion forces[47], or to a combination of these factors. Based on our results in intercalated epitaxial graphene, we can discard meso-nanoscale roughness and adhesion as the main driving forces. Indeed, we measure similar values of surface roughness and adhesion forces across the non-intercalated and intercalated pairs of samples, as reported in Table S2 of the Supplementary Information. Regarding the puckering and e-ph coupling effects, while they certainly play a role, the results here reported clearly indicate that the key parameter controlling friction in epitaxial graphene, and likely other 2D materials, is the interfacial shear modulus. For example, we find that for non-intercalated 2L graphene and H-intercalated 1L graphene the friction behavior is identical, as it is their $G_{int}$. Furthermore, the ratio between $G_{int}$ of 2L and $G_{int}$ of 1L is the same for both non-intercalated and intercalated graphene samples, as it is the ratio of the corresponding friction coefficients. In order to understand the relationship between interfacial shear elasticity and friction, we have developed simple friction models, as discussed in the next paragraph.

**Friction force simulation and discussion**

To simulate the friction force probed by a sliding AFM tip on a surface we first use the simple Prandtl-Tomlinson (PT) model[48,49], where a nano-tip is dragged by a spring over a corrugated energy landscape. In the PT model the total potential energy U(x,t) of the system is described by:

$$U(x,t) = \frac{1}{2} k_{total}^{lateral} \ (x - vt)^2 + V_{tip-layer}(x). \quad (6)$$

Here the first term on the right-hand side represents the potential energy stored in the total lateral spring constant of the tip-contact system, $k_{total}^{lateral}$ (see Eq. 2) when the tip is sliding with velocity v (v = 1 m/s). The second term describes the energy barrier that the tip has to overcome to slide over the periodic lattice of the sample surface, more details are reported in Methods and the SI. As discussed in Equations (1), (2) and (3), the value of $G_{int}$ is directly related to the value $k_{total}^{lateral}$. Here, the PT model is then used to simulate friction forces for samples with different values of $G_{int}$ (see Fig. 5a and SI). Like in the above-reported experimental results, the PT model demonstrates that for higher $G_{int}$ values, steady state friction has lower values, due to a larger amount of energy stored elastically during the sticking regime, and a smaller amount dissipated during slip. This can be easily seen in Fig. 5b (see Fig. S10), where we show the potential energy of the system, see U(x,t) in Eq. 6, represented by a corrugated parabola, as a function of the tip position, for two different values of $G_{int}$. The curves indicate that when the tip starts sliding (slip event) on the sample with larger $G_{int}$, the same tip, for a sample with lower $G_{int}$, still has an energy barrier to overcome before starting to slide. As a consequence, the friction is larger for smaller $G_{int}$.

While this simple PT model immediately rationalizes the experimental results, it is informative to gain a more intimate physical understanding of the dissipation process. To do that, we develop 1D cartoon simulations based on a Frenkel Kontorova (FK) model, where a point tip dragged by a spring with velocity v slides onto a 1D harmonic chain representing the graphene layer, while the chain atoms feel underneath a sinusoidal potential taken with the same spacing as the chain (a commensurate FK model), mimicking the layer-substrate interaction (Fig. 5c). The chain is therefore pinned against sliding, by an amount controlled by the magnitude A of the layer-substrate interfacial potential: weak A represents sliding on the carbon buffer layer, stronger A sliding on H-terminated SiC. The resulting friction force model evolution of Fig 5c shows the initial elastic displacement with overall stiffness $k_{total}^{lateral}$, from which the contact lateral stiffness $k_{cont}^{lateral}$ is extracted (see Eq. 2), followed by atomic stick-slip events. Steady state friction and $k_{cont}^{lateral}$ as a function of A are displayed in Fig. 5d, showing that the same

behavior reported experimentally is reproduced in this model. A larger A yields a larger interfacial shear stiffness and a lower friction, since lesser atoms are displaced and lesser "bonds" with the graphene layer are broken. The displaced atoms need not pucker outwards which will cost a large adhesion energy but will locally slide out of commensurability with the substrate for a limited range. We are thus led to two conclusions. First, interfacial shear stiffness, related to the layer-substrate interfacial energy, controls friction. Second, frictional work, which must comprise an important part from bond breaking, decreases despite the larger layer-substrate interfacial energy between graphene and H-SiC (compared to the Bfl/SiC substrate), because the spatial extent of the distortion decreases for larger values of $G_{int}$.

**Conclusions**

By using the sub-Ångstrom-resolution modulated nanoshear method, we measure the interfacial transverse shear modulus of atomically thin epitaxial graphene layers on SiC. We show that this modulus is a key property of the interface between a single atomic layer and the underlying substrate, and is critically controlled by the chemistry, stacking, and structure of the graphene-substrate interface. Indeed, the experiments show that when H is intercalated between graphene and SiC, the interfacial shear modulus augments, and it is rigidly shifted towards higher values. Furthermore, we find that the interfacial shear modulus increases for bilayer films compared to monolayer films, in both systems, i.e., with and without hydrogen intercalation. The increase of $G_{int}$ for two layers compared to one layer can be related to layer-layer and layer-substrate stacking order, whereas the increase after hydrogen intercalation is explained in terms of the graphene layers being much more pinned by the H-atoms at the interface, compared to the H-free case.

Importantly, the interfacial shear modulus, largely ignored so far, is pivotal to control and predict sliding friction in supported graphene, a topic that has produced a large amount of fundamental yet somewhat controversial studies. In particular, we find that the friction coefficient is inversely related to the interfacial shear modulus, and this result can be easily explained by simple 1D sliding friction models, which show that for larger shear softness, a larger amount of energy is dissipated during sliding while a smaller amount of energy is stored elastically. This picture explains in full the experimental friction results by only considering the shear stiffness, without the need to invoke other effects, such as puckering, or electron-phonon dissipation. These results can be generalized to other 2D materials, and represent a way to control atomic sliding friction.

To conclude, the ability to measure and tune the interfacial shear modulus of a single atomic layer on a substrate has the potential to open new directions in terms of fundamental understanding of atomic interfaces, and in terms of new approaches to manipulate strain fields for band-structure engineering and photonics applications.

## Methods

### Growth and hydrogen intercalation of epitaxial graphene films on SiC:

Large area epitaxial graphene films are grown on the Si-face of on-axis 6H SiC (II-VI Inc.) by thermal Si sublimation in Argon atmosphere, as described in Ref.[25]. The first carbon layer forming from the decomposition of the Si-face of the SiC substrate is a complex interface layer, called the buffer layer (Bfl), which is partially covalently bonded to the SiC surface (Fig. 1b left panel). The successive graphene layers are on top of the buffer layer. Therefore, when we refer to monolayer epitaxial graphene and bilayer epitaxial graphene, we consider one layer and two layers of graphene on top of the buffer layer, respectively. Hydrogen intercalation at the interface between SiC and the Bfl is obtained by means of H annealing of as-grown epitaxial graphene films, to achieve quasi-free-standing graphene films on H-passivated SiC[26,27]. In particular, 1L/H-SiC is obtained from hydrogen intercalation of bare Bfl, while 2L/H-SiC is obtained from hydrogen intercalation of monolayer epitaxial graphene – see Fig. 1b and Fig. S1 in the Supplementary Information for a visual schematic of the crystal structure of the four samples. Raman spectroscopy is used to assess the crystal quality and the number of atomic layers in each of the four samples, and to confirm the successful intercalation of hydrogen and the formation of free-standing graphene – see SI.

### Modulated Nanoindentation (MoNI/Å-I) measurements of E*:

In order to derive the interfacial shear modulus from $k_{cont}^{lateral}$ via Eq. 5, the effective Young's modulus E* needs to be measured. We determine the effective Young's moduli E* of the four graphene samples via AFM-based Modulated Nanoindentation (MoNI/Å-I), performed with an Agilent PicoPlus AFM. A detailed description of the MoNI/Å-I method is provided in the Supplementary Information and it is extensively treated in Refs.[36-38]. Here, we perform MoNI/Å-I indentations with maximum loads of 100 nN and indentation depths ~ 1-2 Å. We remark that these loads are not high enough to activate the graphene-diamene phase transition. Force-indentation curves are acquired on multiple regions (more than 30) of the two non-intercalated and two H-intercalated samples. The effective Young's moduli of the samples are extracted from the force-indentation curves by fitting via the nonlinear Hertz's model[37]. The

four samples exhibit all similar Young's moduli, around 400 GPa (390 GPa for 1L/Bfl/SiC, 363 GPa for 2L/Bfl/SiC, 384 GPa for 1L/H-SiC, and 389 GPa for 2L/H-SiC), which are values similar to the Young's modulus of the SiC substrate[50]. The contact stiffness measured via nanoindentation on supported 2D materials accounts for the elastic response of both the overlying thin 2D layers and the underlying substrate. The results are summarized in Fig. S8 in the SI.

**Interfacial shear modulus and modulated nanoshear measurements:**

A detailed description of the MoNS technique can be found in the Supplementary Information (see Fig. S3). During the interfacial shear modulus measurements, the AFM tip is brought into contact with the sample at a specific normal force, which is controlled by the AFM feedback loop. Sub-angstrom lateral oscillations are applied to the AFM tip-holder via a piezoelectric stage at 2.213 kHz controlled by a Lock-in amplifier while the tip is sticking in contact with the sample surface (no slip). The variation in lateral force at each normal load is recorded during AFM tip retraction from the sample until complete withdrawal from the surface is achieved, at a rate of 0.9 nN/s. We perform MoNS experiments on multiple areas of the four sample surfaces, acquiring 30+ $k^{lateral}_{cont}$ vs $F_N$ curves for each sample (See Fig. S4 in the SI). The interfacial transverse shear moduli $G_{int}$ obtained from the 30+ curves are averaged and summarized in Fig. 3. More details on the technique and the reproducibility of the results are provided in the SI.

**Friction force measurements:**

The friction force measurements are performed on a Brucker Multimode 8 AFM using a silicon AFM probe (PPP-LFMR, Nanosensors, tip radius $R_{tip}$ ~ 10 nm, normal spring constant 0.3 N/m, as measured by the thermal noise method). Topography and friction force maps (1.5 x 1.5 $\mu m^2$) are collected while scanning the tip in contact with the surface of the graphene samples, with a scanning speed of 6 μm/s – see Fig. 4a. Even within this small scanning area, it is possible to find graphene domains of different thickness, as we can see in the bottom/first-from-left panel in Fig. 4a, where we have areas of 1L graphene and areas of 2L graphene in the same scan[29]. We extract the average friction force selectively from the regions of interest of the friction map – highlighted with solid-line boundaries in Fig. 4a. From each sample, we collect friction force maps at different normal loads, from -10 nN to 50 nN, with 10 nN steps. The friction forces reported in the friction curves of Fig. 4b are the average values from different positions. The normalized distribution of the friction force values measured on each sample (for a specific

normal load, 50 nN) is available in Fig. S7. To obtain the friction coefficient μ, for each graphene sample, we fit the respective friction curve using the following nonlinear equation[51]

$$F_L = \mu(F_N + F_{adh})^{2/3}. \quad (7)$$

Here $F_{adh}$ is the adhesion force, and $\mu$ is the friction force coefficient. For more details about the friction experimental set up and results, see SI.

**Computational methods:**

*Prandtl-Tomlinson Model.* The time evolution of the system, as sketched in the inset of Fig. 5a, with the total potential energy (Eq. 6) is obtained from the solution of the equation of motion[48,49]

$$m\ddot{x} = -\frac{dU(x,t)}{dx} - m\eta\dot{x}\,, \quad (8)$$

where $m$ is the mass ($m = 501.40 m_{carbon}$), and η is the damping parameter (η=18.75 $ps^{-1}$)[52]. The total potential is described by Eq. 6, where the $V_{tip\text{-}layer}$ potential is described by the following equation:

$$V_{tip-layer}(x) = V\left(1 - \cos\left[\frac{2\pi}{a}x\right]\right). \quad (9)$$

The friction force is calculated by

$$F_F = k_{total}^{lateral}(X(t) - x(t)), \quad (10)$$

where X(t)=vt is the coordinate of the pulling spring and x(t) is the tip coordinate. The steady state value can be calculated as a time average of the friction force. The numerical solution of Eq. 8 is obtained using a Python code with a time step of 2.5 ps.

*Frenkel-Kontorova Model*. Non equilibrium model molecular dynamics simulations are carried out with a home-made code. As sketched in the inset of Fig. 5c, a one-dimensional chain of 120 particles of mass $m_c$ and first neighbor harmonic potential stiffness $k_0$ (graphene) is sliding on an external rigid sinusoidal potential (the substrate) of amplitude A and same spacing as the chain at rest, i.e., a commensurate Frenkel-Kontorova model. A point tip of mass M is dragged by a spring (spring constant equals to $k_{lever}^{t}$) over the chain. The time evolution of frictional force is obtained by Eq. 10. Friction eventually converges for sufficiently large times and sliding distance to the steady state value of friction. The interfacial shear stiffness $k_{cont}^{lateral}$ is obtained, starting from initially relaxed conditions, from the initial slope of the friction curves in Fig. 5c, using Eq. 2.

**Acknowledgments**

This work is funded by the US Department of Energy, and the Army Research Office.

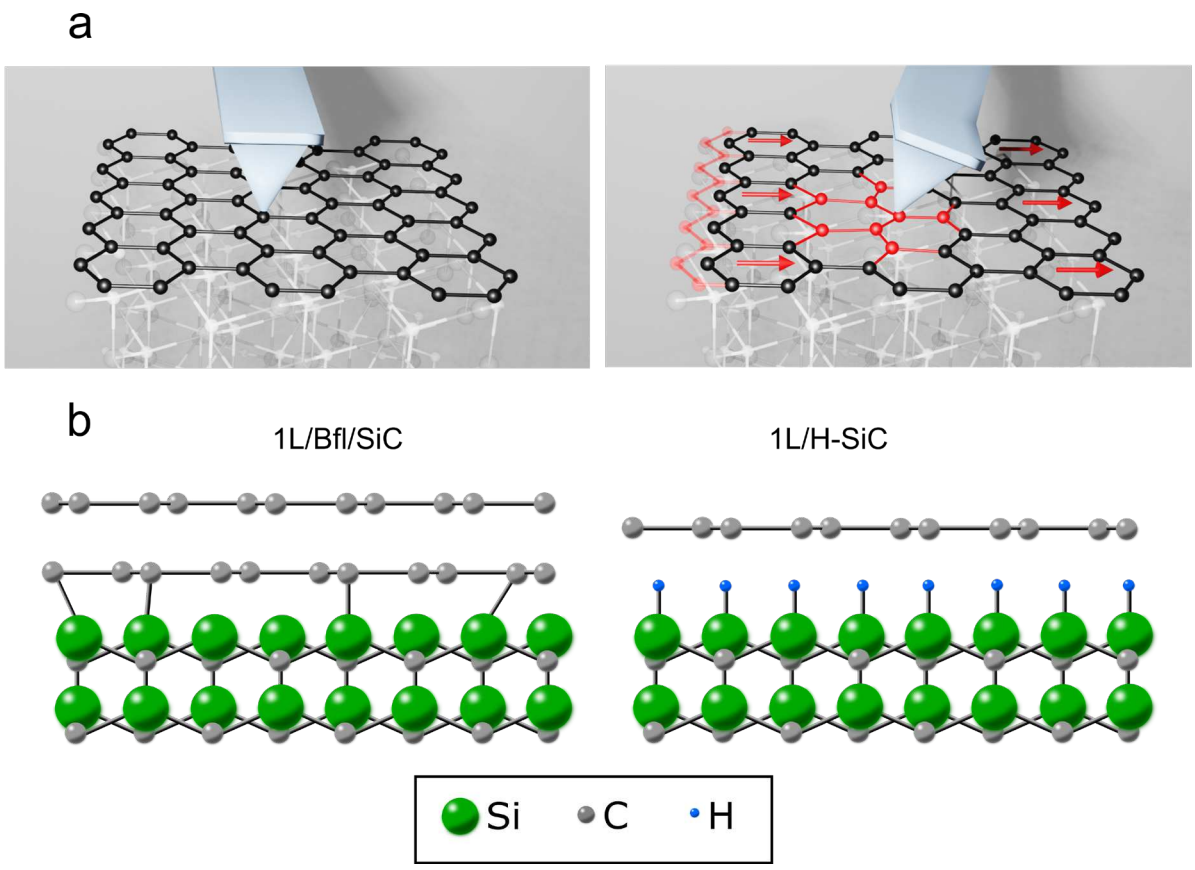


**Figure 1 | Interfacial shear modulus experiment. a)** Scheme of the interfacial shear modulus experiments. Initially, an AFM tip is brought into contact with a graphene layer sitting on a substrate (left panel). The AFM tip is then (right panel) oscillated in-plane while in contact with the graphene surface, causing rigid moving of the graphene atomic layer and/or stretching of the interatomic bonds within the graphene layer, in an elastic regime (no slipping). **b)** Schemes of (left panel) one epitaxial graphene layer on the conventional C-buffer layer on SiC(0001), and (right panel) one quasi free-standing graphene layer on SiC(0001) after hydrogen intercalation.

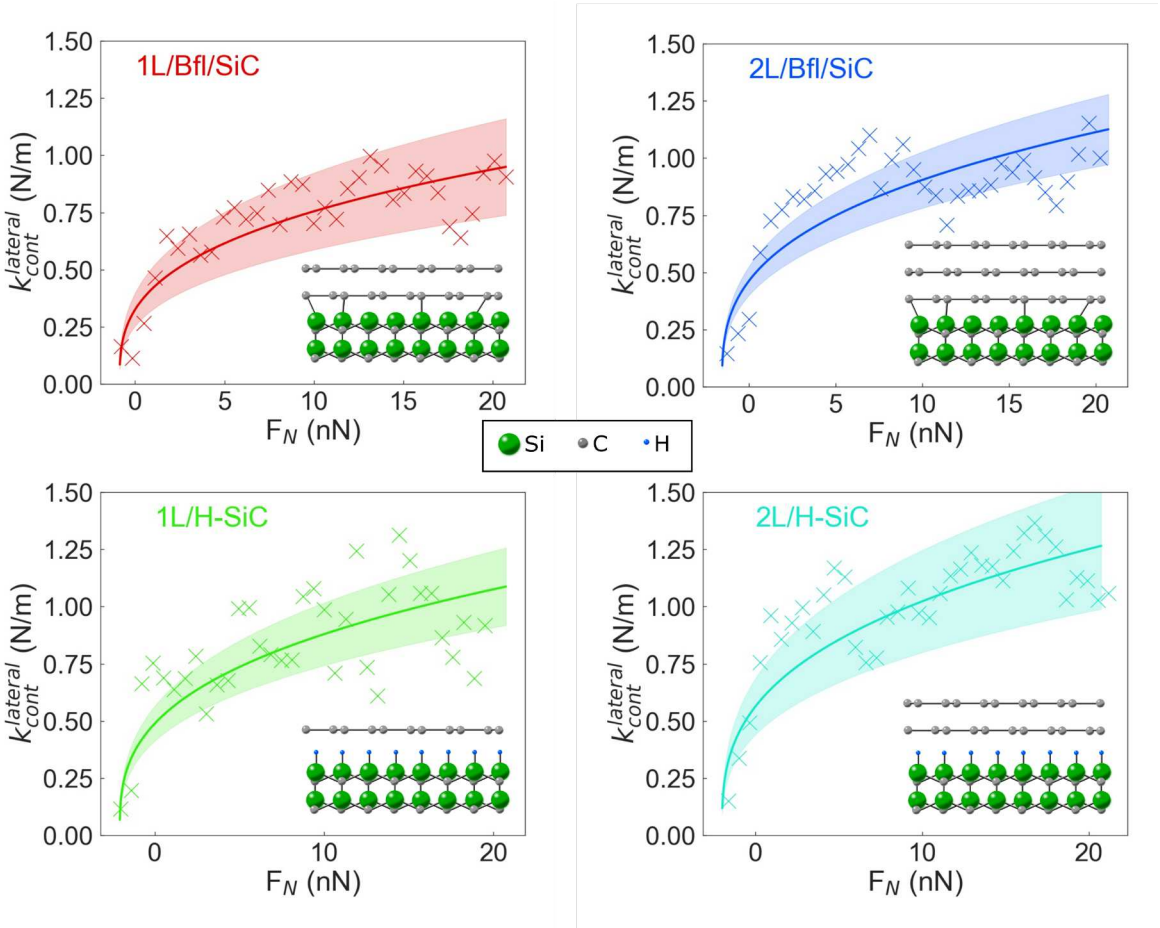


**Figure 2 | Interfacial transverse shear modulus measurements.** Contact stiffness ($k_{cont}^{lateral}$) versus normal load ($F_N$) obtained from the modulated nanoshear measurements, for 1L/Bfl/SiC, 2L/Bfl/SiC, 1L/H-SiC, and 2L/H-SiC. The solid lines represent the nonlinear fitting with Eq. 5, the markers represent data points from a single experiment, and the shaded areas represent the standard deviation for multiple experiments. In the insets, the schematics of the respective crystal arrangement of the four samples.

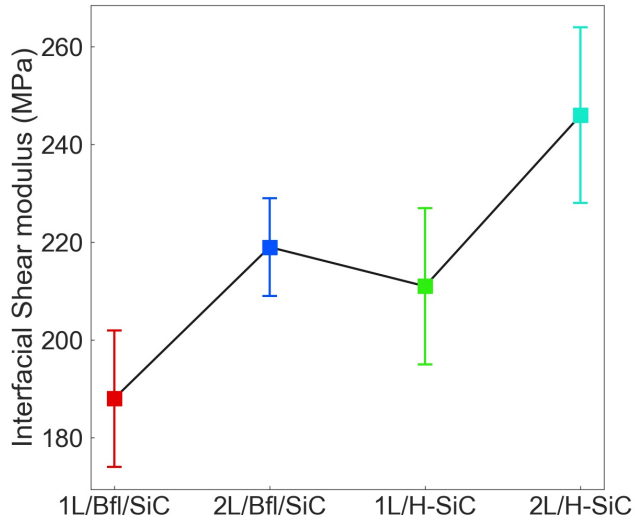


| Graphene | $G_{int}$ (MPa) | $\mu$ ($nN^{1/3}$)$10^{-2}$ |
|---|---|---|
| 1L/Bfl/SiC | 188 | 2.3 |
| 2L/Bfl/SiC | 220 | 1.4 |
| 1L/H-SiC | 211 | 1.4 |
| 2L/H-SiC | 246 | 0.9 |

**Figure 3 | Interfacial transverse shear modulus results. a)** Variation of the interfacial transverse shear modulus extracted from fitting the experimental data in Figure 2, according to Eq. 5, with the respective standard deviations. **b)** Table summarizing the values of the interfacial transverse shear modulus $G_{int}$ and friction coefficient μ for the different graphene samples, with standard deviation errors of 15 MPa and 0.002 $nN^{1/3}$, respectively.

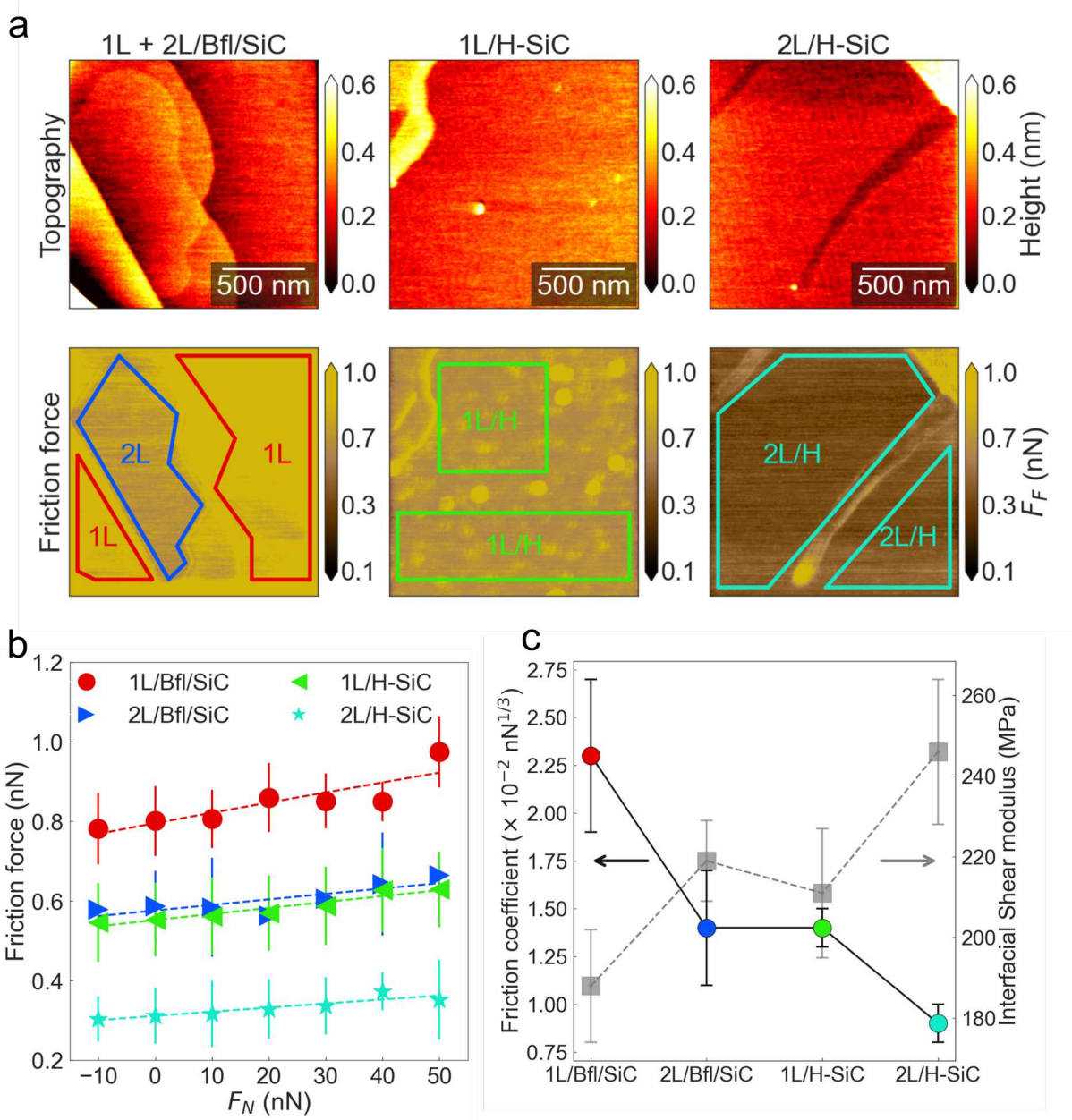


**Figure 4 | Correlation between friction force and interfacial transverse shear modulus. a)** Contact-mode AFM topography maps (top panels) and friction force maps (bottom panels, acquired at 50 nN normal load, same lateral scale as the topography maps) for the two pairs of non-intercalated and H-intercalated graphene samples. The first column shows a sample with areas of 1L graphene and 2L graphene on the buffer layer on SiC. In the second and third column, we present maps of 1L/H-SiC and 2L/H-SiC graphene films, respectively. **b)** Friction force versus normal load for the different graphene samples. Here, friction values are extracted and averaged from the corresponding areas highlighted in the friction maps in (a), marked by solid-line boundaries. The average friction force values are plotted as markers, while the dashed curves represent the theoretical fit with Eq. 7. **c**) Comparison between interlayer transverse shear modulus and friction force coefficient for the two pairs of non-intercalated and H-intercalated graphene samples. The friction coefficients are extracted from fitting the experimental data in (b) with Eq. 7 for 1L/Bfl/SiC ($2.3\times10^{-2}$ nN$^{1/3}$), 2L/Bfl/SiC ($1.4\times10^{-2}$ nN$^{1/3}$), 1L/H-SiC ($1.4\times10^{-2}$ nN$^{1/3}$), and 2L/H-SiC ($0.9\times10^{-2}$ nN$^{1/3}$).

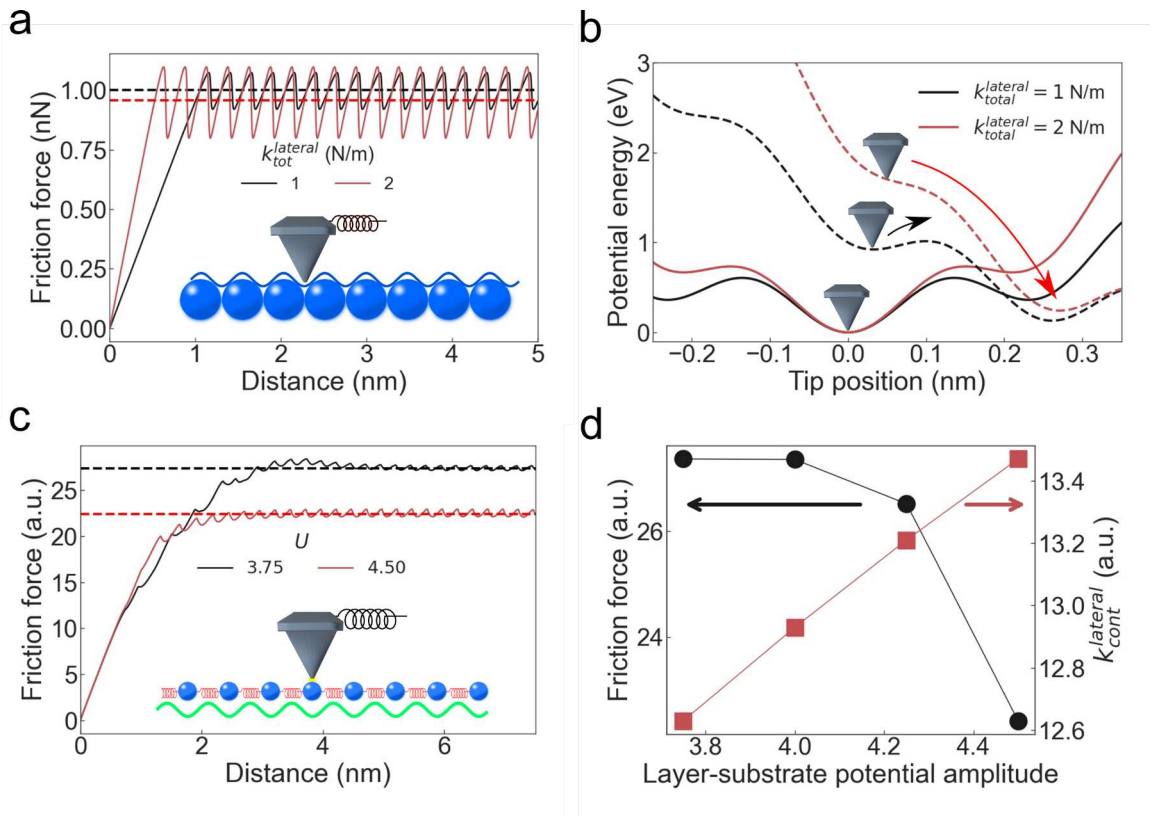


**Figure 5 | Friction force modeling.** a) Prandtl-Tomlinson modeling of the friction forces as a function of tip sliding distance. In the inset a cartoon of the PT model, where the tip slides on a fixed potential representing the graphene plus substrate system. b) PT potential energy (see Eq. 6) as a function of the AFM tip position, according to the PT model. (c) FK modeling of the friction forces as a function of tip sliding distance. In the inset a cartoon of the FK model, where the tip slides on top of a 1D chain of springs (representing the graphene atoms), which moves on top of a fixed potential (representing the graphene-substrate interaction). (d) Sliding friction force and transverse shear stiffness vs. layer-substrate potential amplitude as resulting from the FK model. The inverse relation of the two quantities is similar to experiments

## REFERENCES


1 Li, Q., Lee, C., Carpick, R. W. & Hone, J. Substrate effect on thickness-dependent friction on graphene. *physica status solidi (b)* **247**, 2909-2914, doi:10.1002/pssb.201000555 (2010).

2 Bleu, Y. *et al.* Raman study of the substrate influence on graphene synthesis using a solid carbon source via rapid thermal annealing. *Journal of Raman Spectroscopy* **50**, 1630-1641, doi:10.1002/jrs.5683 (2019).

3 Sun, Y., Wang, R. & Liu, K. Substrate induced changes in atomically thin 2-dimensional semiconductors: Fundamentals, engineering, and applications. *Applied Physics Reviews* **4**, doi:10.1063/1.4974072 (2017).

4 Mammadov, S. *et al.* Work function of graphene multilayers on SiC(0001). *2D Materials* **4**, doi:10.1088/2053-1583/4/1/015043 (2017).

5 Kim, N., Kim, K. S., Jung, N., Brus, L. & Kim, P. Synthesis and electrical characterization of magnetic bilayer graphene intercalate. *Nano Lett* **11**, 860-865, doi:10.1021/nl104228f (2011).

6 Pang, Z. *et al.* Giant tunability of interlayer friction in graphite via ion intercalation. *Extreme Mechanics Letters* **35**, doi:10.1016/j.eml.2019.100616 (2020).

7 Gao, Y. *et al.* Elastic coupling between layers in two-dimensional materials. *Nat Mater* **14**, 714-720, doi:10.1038/nmat4322 (2015).

8 Voiry, D. *et al.* Enhanced catalytic activity in strained chemically exfoliated WS(2) nanosheets for hydrogen evolution. *Nat Mater* **12**, 850-855, doi:10.1038/nmat3700 (2013).

9 Bao, W. *et al.* Approaching the limits of transparency and conductivity in graphitic materials through lithium intercalation. *Nat Commun* **5**, 4224, doi:10.1038/ncomms5224 (2014).

10 Xu, C., Xue, T., Qiu, W. & Kang, Y. Size Effect of the Interfacial Mechanical Behavior of Graphene on a Stretchable Substrate. *ACS Appl Mater Interfaces* **8**, 27099-27106, doi:10.1021/acsami.6b08812 (2016).

11 Jiang, T., Huang, R. & Zhu, Y. Interfacial Sliding and Buckling of Monolayer Graphene on a Stretchable Substrate. *Advanced Functional Materials* **24**, 396-402, doi:10.1002/adfm.201301999 (2014).

12 Cho, J., Luo, J. J. & Daniel, I. M. Mechanical characterization of graphite/epoxy nanocomposites by multi-scale analysis. *Composites Science and Technology* **67**, 2399-2407, doi:10.1016/j.compscitech.2007.01.006 (2007).

13 Seldin, E. J. & Nezbeda, C. W. Elastic Constants and Electron-Microscope Observations of Neutron-Irradiated Compression-Annealed Pyrolytic and Single-Crystal Graphite. *Journal of Applied Physics* **41**, 3389-3400, doi:10.1063/1.1659430 (1970).

14 Savini, G. *et al.* Bending modes, elastic constants and mechanical stability of graphitic systems. *Carbon* **49**, 62-69, doi:10.1016/j.carbon.2010.08.042 (2011).

15 Peng, Z., Chen, X., Fan, Y., Srolovitz, D. J. & Lei, D. Strain engineering of 2D semiconductors and graphene: from strain fields to band-structure tuning and photonic applications. *Light Sci Appl* **9**, 190, doi:10.1038/s41377-020-00421-5 (2020).

16 Kawai, S. *et al.* Superlubricity of graphene nanoribbons on gold surfaces. *Science* **351**, 957-961, doi:10.1126/science.aad3569 (2016).

17 Bunch, J. S. *et al.* Electromechanical Resonators from Graphene Sheets. *Science* **315**, 490-493, doi:10.1126/science.1136836 (2007).

18 Frank, I. W., Tanenbaum, D. M., van der Zande, A. M. & McEuen, P. L. Mechanical properties of suspended graphene sheets. *Journal of Vacuum Science & Technology B: Microelectronics and Nanometer Structures* **25**, doi:10.1116/1.2789446 (2007).

19 Wang, Z. & Feng, P. X. L. Design of black phosphorus 2D nanomechanical resonators by exploiting the intrinsic mechanical anisotropy. *2D Materials* **2**, doi:10.1088/2053-1583/2/2/021001 (2015).

20 Chen, C. *et al.* Performance of monolayer graphene nanomechanical resonators with electrical readout. *Nat Nanotechnol* **4**, 861-867, doi:10.1038/nnano.2009.267 (2009).

21 Glavin, N. R., Muratore, C. & Snure, M. Toward 2D materials for flexible electronics: opportunities and outlook. *Oxford Open Materials Science* **1**, doi:10.1093/oxfmat/itaa002 (2021).
22 Alert, R. & Casademunt, J. Role of Substrate Stiffness in Tissue Spreading: Wetting Transition and Tissue Durotaxis. *Langmuir* **35**, 7571-7577, doi:10.1021/acs.langmuir.8b02037 (2019).
23 Qu, W., Bagchi, S., Chen, X., Chew, H. B. & Ke, C. Bending and interlayer shear moduli of ultrathin boron nitride nanosheet. *Journal of Physics D: Applied Physics* **52**, doi:10.1088/1361-6463/ab3953 (2019).
24 Chen, X., Yi, C. & Ke, C. Bending stiffness and interlayer shear modulus of few-layer graphene. *Applied Physics Letters* **106**, doi:10.1063/1.4915075 (2015).
25 Kunc, J. *et al.* Effect of Residual Gas Composition on Epitaxial Growth of Graphene on SiC. *Physical Review Applied* **8**, doi:ARTN 04401110.1103/PhysRevApplied.8.044011 (2017).
26 Kunc, J., Rejhon, M. & Hlidek, P. Hydrogen intercalation of epitaxial graphene and buffer layer probed by mid-infrared absorption and Raman spectroscopy. *Aip Advances* **8**, doi:Artn 04501510.1063/1.5024132 (2018).
27 Rejhon, M. & Kunc, J. ZO phonon of a buffer layer and Raman mapping of hydrogenated buffer on SiC(0001). *Journal of Raman Spectroscopy* **50**, 465-473, doi:10.1002/jrs.5533 (2018).
28 Filleter, T. & Bennewitz, R. Structural and frictional properties of graphene films on SiC(0001) studied by atomic force microscopy. *Physical Review B* **81**, doi:10.1103/PhysRevB.81.155412 (2010).
29 Filleter, T. *et al.* Friction and dissipation in epitaxial graphene films. *Phys Rev Lett* **102**, 086102, doi:10.1103/PhysRevLett.102.086102 (2009).
30 Lang, H. *et al.* Effect of relative humidity on the frictional properties of graphene at atomic-scale steps. *Carbon* **137**, 519-526, doi:10.1016/j.carbon.2018.05.069 (2018).
31 Lee, C. *et al.* Frictional characteristics of atomically thin sheets. *Science* **328**, 76-80, doi:10.1126/science.1184167 (2010).
32 Li, S. *et al.* The evolving quality of frictional contact with graphene. *Nature* **539**, 541-545, doi:10.1038/nature20135 (2016).
33 Shin, Y. J. *et al.* Frictional characteristics of exfoliated and epitaxial graphene. *Carbon* **49**, 4070-4073, doi:10.1016/j.carbon.2011.05.046 (2011).
34 Zeng, X., Peng, Y. & Lang, H. A novel approach to decrease friction of graphene. *Carbon* **118**, 233-240, doi:10.1016/j.carbon.2017.03.042 (2017).
35 Lavini, F. *et al.* Friction and work function oscillatory behavior for an even and odd number of layers in polycrystalline MoS2. *Nanoscale* **10**, 8304-8312, doi:10.1039/c8nr00238j (2018).
36 Gao, Y. *et al.* Ultrahard carbon film from epitaxial two-layer graphene. *Nat Nanotechnol* **13**, 133-138, doi:10.1038/s41565-017-0023-9 (2018).
37 Cellini, F., Gao, Y. & Riedo, E. Å-Indentation for non-destructive elastic moduli measurements of supported ultra-hard ultra-thin films and nanostructures. *Scientific Reports* **9**, doi:10.1038/s41598-019-40636-0 (2019).
38 Cellini, F. *et al.* Pressure-Induced Formation and Mechanical Properties of 2D Diamond Boron Nitride. *Advanced Science*, 2002541, doi:10.1002/advs.202002541 (2020).
39 Carpick, R. W., Ogletree, D. F. & Salmeron, M. Lateral stiffness: A new nanomechanical measurement for the determination of shear strengths with friction force microscopy. *Applied Physics Letters* **70**, 1548-1550, doi:10.1063/1.118639 (1997).
40 Blakslee, O. L., Proctor, D. G., Seldin, E. J., Spence, G. B. & Weng, T. Elastic Constants of Compression-Annealed Pyrolytic Graphite. *Journal of Applied Physics* **41**, 3373-3382, doi:10.1063/1.1659428 (1970).

41 Xiao, J. R., Gama, B. A. & Gillespie, J. W. An analytical molecular structural mechanics model for the mechanical properties of carbon nanotubes. *International Journal of Solids and Structures* **42**, 3075-3092, doi:10.1016/j.ijsolstr.2004.10.031 (2005).
42 Razado-Colambo, I. *et al.* Structural determination of bilayer graphene on SiC(0001) using synchrotron radiation photoelectron diffraction. *Sci Rep* **8**, 10190, doi:10.1038/s41598-018-28402-0 (2018).
43 Emtsev, K. V., Speck, F., Seyller, T., Ley, L. & Riley, J. D. Interaction, growth, and ordering of epitaxial graphene on SiC{0001} surfaces: A comparative photoelectron spectroscopy study. *Physical Review B* **77**, doi:10.1103/PhysRevB.77.155303 (2008).
44 Speck, F. *et al.* The quasi-free-standing nature of graphene on H-saturated SiC(0001). *Applied Physics Letters* **99**, doi:10.1063/1.3643034 (2011).
45 Lee, K. *et al.* Magnetotransport properties of quasi-free-standing epitaxial graphene bilayer on SiC: evidence for Bernal stacking. *Nano Lett* **11**, 3624-3628, doi:10.1021/nl201430a (2011).
46 Dong, Y. Effects of substrate roughness and electron–phonon coupling on thickness-dependent friction of graphene. *Journal of Physics D: Applied Physics* **47**, doi:10.1088/0022-3727/47/5/055305 (2014).
47 Deng, Z., Smolyanitsky, A., Li, Q., Feng, X. Q. & Cannara, R. J. Adhesion-dependent negative friction coefficient on chemically modified graphite at the nanoscale. *Nat Mater* **11**, 1032-1037, doi:10.1038/nmat3452 (2012).
48 Tomlinson, G. A. CVI. A molecular theory of friction. *The London, Edinburgh, and Dublin Philosophical Magazine and Journal of Science* **7**, 905-939, doi:10.1080/14786440608564819 (1929).
49 Prandtl, L. Ein Gedankenmodell zur kinetischen Theorie der festen Körper. *ZAMM - Zeitschrift für Angewandte Mathematik und Mechanik* **8**, 85-106, doi:10.1002/zamm.19280080202 (1928).
50 Kitahara, H. *et al.* Mechanical Behavior of Single Crystalline and Polycrystalline Silicon Carbides Evaluated by Vickers Indentation. *Journal of the Ceramic Society of Japan* **109**, 602-606, doi:10.2109/jcersj.109.1271_602 (2001).
51 Riedo, E., Palaci, I., Boragno, C. & Brune, H. The2/3Power Law Dependence of Capillary Force on Normal Load in Nanoscopic Friction. *The Journal of Physical Chemistry B* **108**, 5324-5328, doi:10.1021/jp0360624 (2004).
52 Andersson, D. & De Wijn, A. S. Understanding the friction of atomically thin layered materials. *Nature Communications* **11**, doi:10.1038/s41467-019-14239-2 (2020).

# Supplementary Files

This is a list of supplementary files associated with this preprint. Click to download.

- SIInterfacialShearattheAtomicScale.docx